Macromolecules
ARTICLE

Macromolecules **2010**, *43*, 6213–6224 **6213**
DOI: 10.1021/ma100861b

From Dendrimers to Dendronized Polymers and Forests: Scaling Theory and its Limitations

Martin Kröger,*,† Orit Peleg,† and Avraham Halperin‡

†*Polymer Physics, ETH Zürich, Department of Materials, CH-8093 Zürich, Switzerland, and*
‡*Laboratoire de Spectrométrie Physique (LSP) CNRS UniVersité Joseph Fourier, BP 87, 38402 Saint Martin d'Hères cedex, France*

Received April 19, 2010; Revised Manuscript Received May 26, 2010

ABSTRACT: A unified Flory-type theory of dendron brushes, dendrimers, dendronized polymers, and forests yields scaling rules, state diagrams and information on the collapse transition. The theory also describes the corresponding brushes of linear chains: stars, bottle brushes, and planar brushes. It thus permits a detailed discussion of various tuning parameters and their effects for the different brush types. The discussion addresses the effects of solvent quality, grafting density, the persistence length, and branching functionality. The theory is formulated for the case of "identical monomers" assuming that spacer monomers, junctions, and ends are identical in shape and interactions.

I. Introduction

Regularly branched dendron chains can be attached to a point, a line, or a surface thus giving rise to dendrimers, dendronized polymers (DP), and dendronized surfaces known as forests.[1−6] These are the counterparts of star polymers, bottle-brushes and planar brushes as obtained from terminally anchored linear chains. In dendron brushes, as in brushes of linear polymers, the chains stretch out to reduce the monomer density and the associated free energy penalty. However, the two types of brushes differ in a number of respects: Simple brushes consist of single type of monomer, end effects are negligible and the polymerization degree has no upper limit. In contrast, dendron brushes comprise junction and spacer monomers, end effects are important and the polymerization degree is bound. For simple brushes the polymerization degree N describes the linear chains. The properties of dendron brushes reflect the number of junctions n and their functionality, X, the length of the spacers, s, and the generation of the dendron, g, i.e., the smallest number of junctions joining the root and terminal monomer (see Figure 1). The multiplicity of tuning parameters motivates the development of a phenomenological theory relating the structure to observable properties such as dimensions. The simplest approach is based on a Flory type free energy, a method that yielded a successful description of dendrimers[7−10] and enabled extension to dendronized polymers.[11]

In the following, we reformulate the Flory type theory of dendrimers and DP[7,11] so as to obtain a unified description of the three types of dendronized and linear brushes i.e., brushes grafted to a point, a surface of dimensionality $m = 0$, to a line $m = 1$, or to a planar surface, $m = 2$. This formulation brings out the similarities and differences between the three architectures for the two families of brushes. For each system, it addresses three groups of issues: (i) geometric characteristics such the maximal attainable generation, g_{max} and their dependence on m; (ii) scaling laws characterizing the dependence of dendron size on dendron parameters X, g, s, n, etc. (Table 1); (iii) the collapse behavior of dendron brushes within the Flory approximation. Our primary results concern the three groups of dendronized brushes-dendrimers, dendronized polymers and forests-but these reduce to their "simple brush" counterparts for the proper choice of parameters. Importantly the theory allows to compare between the scaling laws for different solvent qualities and between the boundaries of the scaling regimes as they occur for each of the systems. While it recovers earlier results, on dendron brushes and brushes of linear chains, it also yields new ones such as the scaling laws for forests in general and for dendronized polymers at the Θ temperature. Importantly, at the Θ temperature it is necessary to distinguish between Gaussian, Θ_g, and swollen, Θ_s, subregimes. In the Θ_g the

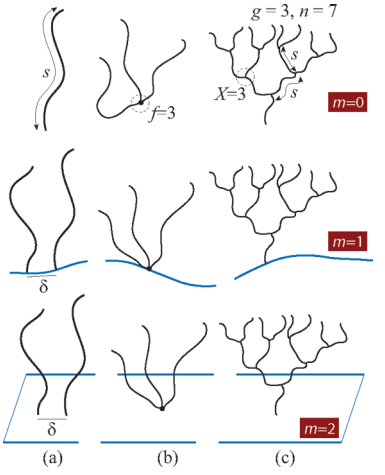

Figure 1. Different dendrons brushes considered in this manuscript and their linear chains counterparts: tethered to $m = 0$ (point), $m = 1$ (line), and $m = 2$-dimensional surfaces. Dendrons have n junctions distributed over g generations, an f-functional root monomer, their mean lateral distance is denoted as δ. Linear chains (a) and f-functional stars (b) are special cases of dendrons (c) with $g = 1$, $n = 1$ and $n = f$, respectively. Linear chains, and spacer chains comprising s monomers are considered semiflexible with persistence length $l_p = pb$, where b is the size of a monomer and p the number of monomers in a persistent segment (b and p not explicitly shown).

*Corresponding author. E-mail: mk@mat.ethz.ch. Fax +41 44 6321076. Telephone +41 44 6326622. Website: http://www.complexfluids.ethz.ch.

Published on Web 06/16/2010

Table 1. Scaling Laws of R_{eq}/b for Dendrimers ($m = 0$), Dendronized Polymers (DP) ($m = 1$), and Dendron Forests ($m = 2$) under Good, Θ_s and Poor Solvent Conditions[a]

m-dimens surface	good solvent ($\tau > 0$)	Θ_s solvent (τ either sign)	poor solvent ($\tau < 0$)	system
$m = 0$	$s^{3/5}(p\tau)^{1/5}$	*) $s^{1/2}p^{1/2}$	$s^{1/3}\lvert\tau\rvert^{-1/3}$	linear chain
point	$f^{1/5}s^{3/5}(p\tau)^{1/5}$	$f^{1/4}s^{1/2}p^{1/8}$	$f^{1/3}s^{1/3}\lvert\tau\rvert^{-1/3}$	star
	$n^{1/5}g^{2/5}s^{3/5}(p\tau)^{1/5}$	$n^{1/4}g^{1/4}s^{1/2}p^{1/8}$	$n^{1/3}s^{1/3}\lvert\tau\rvert^{-1/3}$	dendrimer
	$(\tau R_{min}{}^3R_0{}^2R_{max}/b)^{1/5}$	$(R_{min}{}^6R_0{}^2R_{max}/b)^{1/8}$	$R_{min}\tau\rvert^{-1/3}$	any
$m = 1$	$s^{3/4}(p\tau)^{1/4}(\delta/b)^{-1/4}$	$s^{2/3}p^{1/6}(\delta/b)^{-1/3}$	$s^{1/2}\lvert\tau\rvert^{-1/2}(\delta/b)^{-1/2}$	bottlebrush
line	$n^{1/4}g^{1/2}s^{3/4}(p\tau)^{1/4}(\delta/b)^{-1/4}$	$n^{1/3}g^{1/3}s^{2/3}p^{1/6}(\delta/b)^{-1/3}$	$n^{1/2}s^{1/2}\lvert\tau\rvert^{-1/2}(\delta/b)^{-1/2}$	DP
	$(\tau R_{min}{}^2R_0{}^2R_{max}/b)^{1/4}$	$(R_{min}{}^4R_0{}^2R_{max}/b)^{1/6}$	$R_{min}\lvert\tau\rvert^{-1/2}$	any
$m = 2$	$s(p\tau)^{1/3}(\delta/b)^{-2/3}$	$s(p\tau)^{1/4}(\delta/b)^{-1}$	$s\lvert\tau\rvert^{-1}(\delta/b)^{-2}$	planar brush
plane	$n^{1/3}g^{2/3}s(p\tau)^{1/3}(\delta/b)^{-2/3}$	$n^{1/2}g^{1/2}sp^{1/4}(\delta/b)^{-1}$	$ns\lvert\tau\rvert^{-1}(\delta/b)^{-2}$	dendron forest
	$(\tau R_{min}R_0{}^2R_{max}/b)^{1/3}$	$(R_{min}{}^2R_0{}^2R_{max}/b)^{1/4}$	$R_{min}\lvert\tau\rvert^{-1}$	any

[a] Results for semiflexible linear chains comprising s monomers, bottlebrushes, and planar brushes are contained as the special case of $n = 1, g = 1$, and also tabulated. Results for stars ($m = 0$) with side chains of length s are obtained from the more general result for dendrimers upon choosing $n = f$ and $g = 1$. p denotes the number of monomers in a persistent segment of the spacer chain, or of the linear chain in the absence of junctions. The three characteristic sizes R_{min}, R_0, and R_{max} correspond to the (grafted) collapsed, ideal, and maximum stretched state, respectively. The Θ_g regime with $R_{eq}^{\Theta_g}/b = R_0/b = s^{1/2}g^{1/2}p^{1/2}$ is not listed separately, except for free linear chains. The system labeled with an asterisk cannot exhibit Θ_s scaling (cf. Appendix B); mentioned is the Θ_g scaling. All scaling laws hold within a limited range as discussed in Appendix B.

chains are Gaussian while in the Θ_s they are swollen because of ternary monomer−monomer interactions. Apart from these "habitual" outcomes our analysis of the scaling regimes highlights distinctive problems facing the study of scaling effects in dendron brushes. These problems are traceable to three origins: (i) Dendron scaling laws are applicable in a relatively narrow parameter range. (ii) These scaling windows can be separated by extended crossover regions displaying no simple scaling behavior. (iii) The scaling laws of the simplest, "homopolymer" dendron brushes depend on a number of scaling variables. This is in contrast to linear homopolymers controlled by a single scaling variable, the polymerization degree N. It is thus challenging, as we shall discuss, to distinguish different scaling laws without judicious variation of parameters such as X. Following the majority of earlier theories,[7−9,11] our discussion focuses on the "single monomer approximation" assuming that all monomer species have identical dimensions and that their interactions are described by identical virial coefficients. This description is strictly applicable only to computer simulations where the underlying assumptions can be imposed. However, it provides qualitatively useful insights on dendron brushes in general and serves as a basis for the formulation of more detailed theories distinguishing between the different monomeric species. These results are of interest in view of the intense experimental activity in this area[12−34] and the growing number of simulation[10,27,35−53] and theory[11,27,36,54−57] efforts concerning dendronized systems.

In section II we recall structural aspects of dendronized brushes, including the number of free ends, n_e, characteristic length scales and the maximal attainable generation due to packing constraints, g_{max}. We discuss three important length scales, R_{max}, R_0 and a R_{min} corresponding to a fully extended strand, to a Gaussian strand and to a collapsed, grafted dendron. These enable a unified formulation of scaling laws and the boundaries of the scaling regimes as well as deciding the relevance of free energy terms. A scaling theory of dendronized brushes is described in section III. It is obtained from the free energy per strand allowing for the strand elasticity as well as for binary and ternary monomer−monomer interactions. The boundaries of the different scaling regimes for good, Θ and poor solvent are discussed in section IV where we distinguish between Gaussian Θ_g and swollen Θ_s regimes. Section V is devoted to a discussion of the collapse behavior using a modification of the approach of Birshtein−Pryamitsyn[58] and Fixman.[59] The consequences with regard to the design of simulations and experiments are outlined in Section VI.

II. Dendron Structure: Free Ends, Length Scales, and g_{max}

Certain aspects of dendron behavior are dominated by structural and "geometric" features. These features include two groups of quantities. One is the number of different types of monomers, junctions, n, free ends, n_e and total number of monomers, ns. The second group consists of three characteristic length scales R_{max}, R_0, and R_{min} corresponding respectively to a fully extended strand, a Gaussian strand, and a collapsed, close packed grafted dendron. The three R's play multiple roles in our subsequent discussion. The ratio R_{max}/R_{min} measures the possible range of variation in the size of dendron brushes and the maximal attainable generation g_{max} is specified by $R_{max}/R_{min} = 1$. The ratio R_0/R_{min} provides information on the relevance of the confinement free energy for collapse. Finally, the combination of the three R's enables a compact formulation of our scaling laws and convenient method for comparative plots of scaling regimes.

The "first" monomer of the dendron, the root, is assigned a functionality f. When anchored to a line or surface the grafting density is characterized by the distance between anchors, δ. The grafting density is thus $1/\delta$ or $1/\delta^2$. In the following, we focus on dendron brushes, assuming that δ is small in comparison to the span of a free dendron. For the case of poor solvent, this implies that δ is small in comparison to the size of a collapsed, dense, free dendron. In our discussion of dendronized polymers we consider locally rigid backbone resulting in cylindrical symmetry. A first generation dendron is obtained by reacting the f functionalities with junction monomers having functionality X. Note that f counts the number of sites reacting with junctions. In dendronized polymers additional two functionalities are utilized to create the backbone while in forests an additional functionality anchors the dendron to the surface. The creation of second generation dendrons involves reacting the $f(X - 1)$ free junction functionalities with X-functional junctions and so on. In the general case both the junction-junction and junction-root bonds incorporate a spacer chain comprising s units. The number of junctions grows by a factor $X - 1$ in each generation. Accordingly the total number of junctions is the sum of a geometric series, $n = f + f(X - 1) + f(X - 1)^2 + ...$,

$$n = \frac{f[(X-1)^g - 1]}{(X-2)} \tag{1}$$

Note that eq 1 applies when each reaction is carried out to completion. Importantly, the fraction of free ends among junctions is

$$\frac{n_e}{n} = \frac{(X-2)+f/n}{(X-1)} \geq \frac{X-2}{X-1} \tag{2}$$

Thus, $n_e/n > 1/2$ when $X \geq 3$ and end effects are not negligible for dendrons. Note however that the fraction of free ends among the total number of monomers, including spacers but excluding the root, is n_e/ns and thus smaller.

The volume per dendron within a brush of crowded dendrons is

$$V \simeq \delta^m R^{3-m} \tag{3}$$

where R is the span of the dendron along the normal to the grafting surface and m is the dimensionality of the grafting "surface", i.e., $m = 0, 1, 2$ corresponding respectively to a point, a line and a surface. Accordingly, the average monomer volume fraction is

$$\phi \equiv \frac{nsb^3}{V} \simeq \frac{nsb^3}{\delta^m R^{3-m}} < 1 \tag{4}$$

where nsb^3 is the volume occupied by a densely packed dendron. As noted earlier, we consider all monomers, junctions, free ends, and spacers as identical spheres of diameter b.

The size of the dendron is determined by the span of the strand joining the root with a terminal monomer. A key feature of dendrons arises because the number of monomers increases exponentially, as $(X-1)^g$, while the maximal span of the dendron, as estimated by the length of fully stretched strand

$$R_{\max} = gsb \tag{5}$$

increases linearly with g. The minimal possible span of a dense dendron brush corresponds to $\phi = 1$

$$R_{\min} = b\left[\frac{ns}{(\delta/b)^m}\right]^{1/(3-m)} \tag{6}$$

Note that in our discussion the monomer diameter in eq 6 is identical to the bond length in eq 5, though the two may actually differ. The range of size variation of dendron brushes as the solvent quality is varied is bound by

$$\frac{R_{\max}}{R_{\min}} = \frac{gs}{(ns)^{1/(3-m)}}\left(\frac{\delta}{b}\right)^{m/(3-m)} = \begin{cases} n^{-1/3}gs^{2/3} & m = 0 \\ n^{-1/2}gs^{1/2}(\delta/b) & m = 1 \\ n^{-1}g(\delta/b)^2 & m = 2 \end{cases} \tag{7}$$

The ratio $R_{\max}/R_{\min}$ characterizes the maximal possible difference between swollen and collapsed chains grafted to a m-dimensional surface. In contrast to linear chains and their brushes, $R_{\max}/R_{\min}$ of dendron brushes ultimately decreases with g and eventually reaches unity. This ratio exhibits a maximum (Figure 2) because $R_{\min}$ grows exponentially with g, while $R_{\max}$ increases only linearly. The condition $R_{\min} = R_{\max}$ defines $g_{\max}$, the maximal attainable g. Assuming $g_{\max} \gg 1$ and thus $g_{\max} \gg \ln g_{\max}$ leads to

$$g_{\max} \approx 1 + \frac{\ln[(X-2)s^{2-m}(\delta/b)^m/f]}{\ln(X-1)} \tag{8}$$

and the maximum number of junctions compatible with packing constraint is $n_{\max} \approx f[(X-1)^{g_{\max}} - 1]/(X-2)$. Note that eq 8 underestimates $g_{\max}$ as compared to the value obtained numerically from $R_{\min} = R_{\max}$. In every case, $g_{\max}$ and $R_{\max}/R_{\min}$

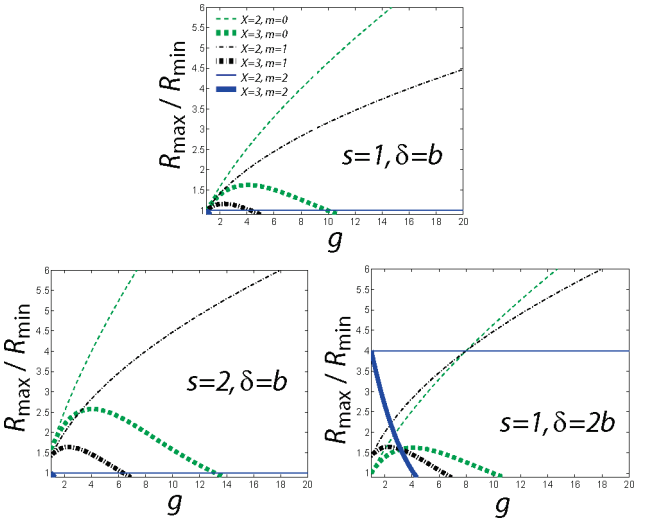

Figure 2. Ratio $R_{\max}/R_{\min}$ vs generation g for dendrons incorporating fully flexible spacers ($p = 1$) at three different choices of spacer length and tethering density. Each graph shows the ratio for both linear chains ($X = 2, f = 1$) and $X = 3$-functional dendrons ($f = 1$), and for all three surface dimensionalities $m = 0, 1, 2$. Some of the $X = 3$ curves for $m = 2$ are hardly visible, signaling the absence of geometrical possibility to create the corresponding structures.

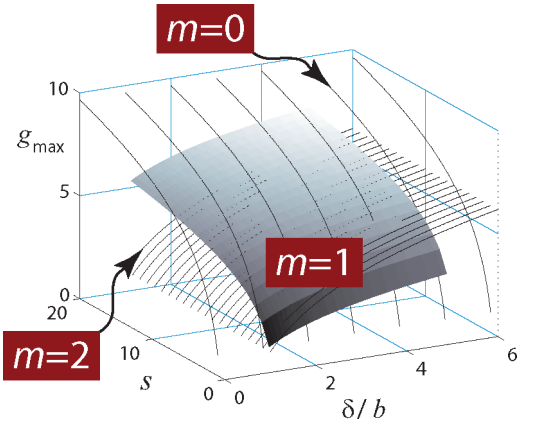

Figure 3. Maximum attainable generation, $g_{\max}$, for $m = 1, 2, 3$ as a function of s and δ/b for the case $X = 3$ and $f = 1$.

decrease as the functionality $X > 2$ increases. It is possible to increase $g_{\max}$ and $R_{\max}/R_{\min}$ by increasing s or δ (Figure 3). However, s is a tuning parameter only for dendrimers, $m = 0$, and DP, $m = 1$, while δ is a control parameter for DP and forests, $m = 2$.

A second ratio of interest is

$$\frac{R_{\min}}{R_0} = \frac{(ns)^{1/(3-m)}}{(gsp)^{1/2}}\left(\frac{b}{\delta}\right)^{m/(3-m)} = \begin{cases} n^{1/3}g^{-1/2}s^{-1/6}p^{-1/2} & m = 0 \\ n^{1/2}g^{-1/2}(p\delta/b)^{-1/2} & m = 1 \\ ng^{-1/2}(s/p)^{1/2}(\delta/b)^{-2} & m = 2 \end{cases} \tag{9}$$

Here R_0 is the Gaussian span of a semiflexible strand as given by

$$R_0 = (gsp)^{1/2}b \tag{10}$$

where $p \approx l_p/b \ll s$ is the number of monomers in a persistent segment of length l_p. $R_{\min}/R_0$ is an indicator for the possibility of a

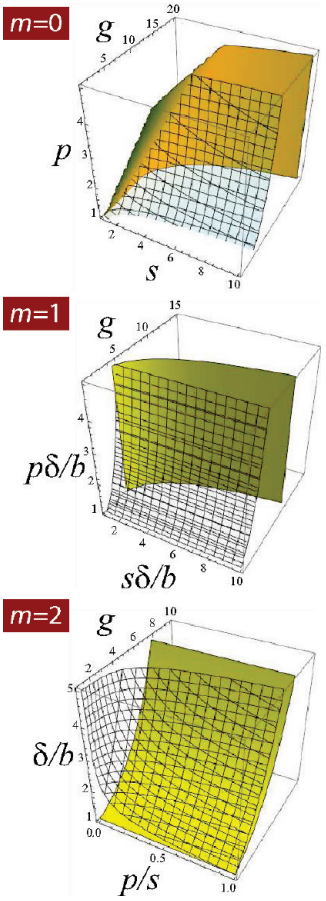

Figure 4. The $R_{min} = R_0$ (transparent lattice) and $R_{min} = R_{max}$ (opaque colored) surfaces for $m = 1, 2, 3$ in the case $X = 3$ and $f = 1$. While the parameters and their range vary with m, all plots depict the width of the $R_{min} < R_0 < R_{max}$ region, confined between the two surfaces, and its dependence g, s, and p. Note that the plot does not include the surface delineating the underlying assumption $R_{min} \gg \delta$.

collapse transition as discussed in section V. It is also helpful in setting the form of the elastic entropy invoked for discussing the collapse behavior. R_{min} of dendron brushes is often larger than R_0 and in such cases the confinement term of the elastic free energy does not play a role. The surfaces corresponding to $R_{min} = R_{max}$ and $R_{min} = R_0$ are depicted in Figure 4 showing that the $R_{min} < R_0 < R_{max}$ region broadens with s and narrows with increasing p.

As noted before and will be discussed later, it is possible to express our scaling results in terms of R_{max}, R_{min}, R_0, given by eqs 5, 6, and 10. Accordingly, the variables g, n, and s appear via the combination gs or ns in all results as exemplified by eqs 7 and 9. It is further useful to note that only R_0 depends on p while the δ dependence is limited to R_{min} (Appendix A). Note further these expressions reproduce the behavior of linear chains and their brushes upon setting $g = 1$, $n = f$, and identifying the number of monomers in a grafted chain with s.[60] In these systems $f = 1$ except for star polymers where $f > 1$ is the number of arms.

III. Scaling Behavior

The span of a dendron brush is determined by the end-to-end distance of a strand joining the root to a terminal monomer. Accordingly the equilibrium state corresponds to a minimum in the free energy per swollen strand.[7] For the purposes of scaling analysis the free energy per strand F_{strand} comprises three terms: $F_{el}/kT \simeq (R/R_0)^2$ specifies the Gaussian stretching penalty, $F_{binary}/kT = vcgs/p \simeq \tau\phi gs$ allows for binary interactions between persistent segments for a strand comprising gs/p persistent segments and $F_{ternary}/kT = wc^2gs/p \simeq \phi^2 gs$ reflects the corresponding ternary interactions. Here, c is the concentration of *persistent* segments, ϕ is the monomer volume fraction and $\tau = (T - \Theta)/T$ is a reduced temperature characterizing the deviation from Θ temperature and setting the sign of F_{binary}. The second and third virial coefficients of interactions between persistent segments comprising p monomers are $v = \tau l_p^2 b \approx \tau p^2 b^3$ and $w = l_p^3 b^3 \approx p^3 b^6$. Altogether

$$\frac{F_{strand}}{k_B T} \simeq \left(\frac{R}{R_0}\right)^2 + \frac{vngs^2}{\delta^m R^{3-m} p^2} + \frac{wn^2 gs^3}{\delta^{2m} R^{6-2m} p^3} \qquad (11)$$

Note that eq 11 does not enable a discussion of the possibility of a collapse transitions because the F_{el} utilized does not allow for confinement. However, this limitation does not affect the collapse scaling laws we will obtain, as determined by the interplay of F_{binary} and $F_{ternary}$. A generalized F_{el}, allowing for both swelling and confinement, is discussed in section V dealing with the collapse behavior.

The equilibrium state is specified by minimization of F_{strand} with respect to R. Since the three terms contain powers of R, the equilibrium scaling behavior can be obtained by equating the relevant free energy terms. The good solvent case corresponds to $F_{binary} \simeq F_{el}$, the swollen Θ regime, Θ_s, to $F_{ternary} \simeq F_{el}$,[8] and the poor solvent case to $F_{binary} \simeq -F_{ternary}$. The Θ_s regime corresponds dendron brushes swollen because of ternary interactions, irrespective of the sign of τ. This regime has no counterpart for free linear chains. In addition, when F_{el} is large compared with both interaction terms, the equilibrium size coincides with that of an undisturbed Gaussian coil, R_0 (see also section V), a regime we denote by Θ_g. As we shall see for dendron brushes the boundaries of the Θ_s regime are wider in comparison to the Θ_g regime (see also Appendix B3). As for linear chains, good solvent implies $\tau > 0$ while poor solvent occurs for $\tau < 0$. The importance of the interaction terms is graded by their value at $R = R_0$ where $F_{el}(R_0) = k_B T$. In terms of the triple R we have

$$\frac{F_{binary}(R_0)}{k_B T} \simeq \tau \left(\frac{R_{min}}{R_0}\right)^{3-m} \frac{R_{max}}{b} \qquad (12)$$

$$\frac{F_{ternary}(R_0)}{k_B T} \simeq \left(\frac{R_{min}}{R_0}\right)^{6-2m} \frac{R_{max}}{b} \qquad (13)$$

where $(R_{min}/R_0)^{3-m}$ is the ratio between volumes occupied at R_{min} and at R_0. Accordingly $F_{binary}(R_0)/F_{ternary}(R_0) \simeq \tau(R_0/R_{min})^{3-m}$ and $F_{ternary}$ is dominant when $\tau < (R_{min}/R_0)^{3-m}$. For the good and Θ_s solvents regimes the equilibrium span of the strands exceeds R_0 since the interaction free energy is larger than $k_B T$.

Altogether the good solvent regime is specified by $F_{binary}(R_0) \gg F_{ternary}(R_0)$ and $F_{binary}(R_0) \gg k_B T$, yielding

$$R_{eq}^{good} \simeq b[\tau n g^2 s^3 p (b/\delta)^m]^{1/(5-m)}$$

$$= \begin{cases} b\tau^{1/5} n^{1/5} g^{2/5} s^{3/5} p^{1/5} & m = 0 \\ b\tau^{1/4} n^{1/4} g^{1/2} s^{3/4} p^{1/4} (b/\delta)^{1/4} & m = 1 \\ b\tau^{1/3} n^{1/3} g^{2/3} s p^{1/3} (b/\delta)^{2/3} & m = 2 \end{cases} \qquad (14)$$

or $R_{eq}^{good} \simeq (\tau {R_{min}}^{3-m} {R_0}^2 R_{max}/b)^{1/(5-m)}$ (see Appendix A). The Θ_s solvent behavior requires $F_{ternary}(R_0) \gg F_{binary}(R_0) > -k_B T$

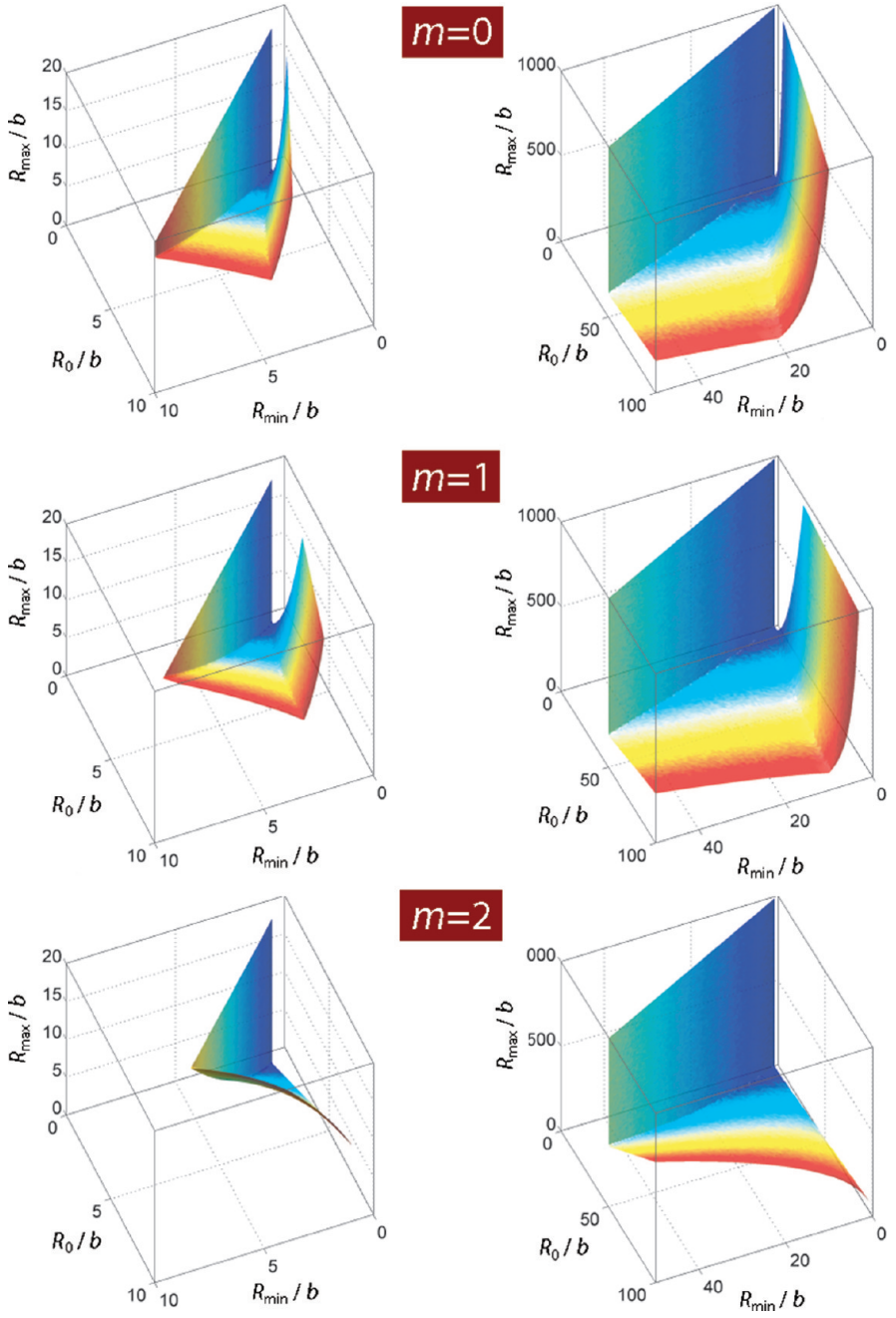

Figure 5. Triple R state diagrams for $\tau = 1$ and all three surface dimensionalities (row 1, $m = 0$; row 2, $m = 1$; row 3, $m = 2$). The left-hand side provides a zoom into the regime of small sizes R from the triple R diagrams shown on the right. The ranges are chosen to capture systems of dendrons, on the left, and of linear chains, right. With increasing surface dimensionality, the good solvent scaling window extends to smaller R_{min} and tends to require larger R_{max}. Not shown in this figure are the remaining scaling regimes, regions forbidden due to packing constraints ($R_{max} > R_{min}$), and regions where scaling is absent. The construction of these triple R state diagram from inequalities G1-G4 is demonstrated, for $\tau = {}^1/_2$, in Figure 6. The theory applies to the regime $R_0 > \delta$, the coloring is therefore chosen to depend on R_0/b alone.

and $F_{ternary}(R_0) \gg k_BT$, leading to

$$R_{eq}^{\Theta_s} \simeq b[n^2 g^2 s^4 p (b/\delta)^{2m}]^{1/(8-2m)} = \begin{cases} bn^{1/4} g^{1/4} s^{1/2} p^{1/8} & m = 0 \\ bn^{1/3} g^{1/3} s^{2/3} p^{1/6} (b/\delta)^{1/3} & m = 1 \\ bn^{1/2} g^{1/2} s p^{1/4} (b/\delta) & m = 2 \end{cases} \quad (15)$$

or $R_{eq}^{\Theta_s} \simeq (R_{min}{}^{6-2m} R_0{}^2 R_{max}/b)^{1/(8-2m)}$. The Θ_g regime, with ideal chain dimensions, is obtained when the interaction terms are too weak to disturb the elastic term, i.e., if $|F_{binary}(R_0)| \ll k_BT$ and $F_{ternary}(R_0) \ll k_BT$,

$$R_{eq}^{\Theta_g} \simeq R_0, \quad (\text{all } m) \quad (16)$$

The poor solvent regime with $F_{binary}(R_0) < -k_BT$ leads to

$$R_{eq}^{poor} \simeq \frac{R_{min}}{(-\tau)^{1/(3-m)}} \quad (17)$$

and is thus restricted to $-1 \le \tau \le 0$ to ensure $R_{eq}^{poor} > R_{min}$. Notice that $R_{eq}^{good} > R_{eq}^{\Theta_s} > R_{eq}^{\Theta_g} > R_{eq}^{poor}$, if the inequalities

defining the regimes are fulfilled. The ordering is not obvious from the scaling forms but can be seen upon expressing eqs 12 and 13 in terms of the equilibrium sizes: $F_{\text{binary}}(R_0)/k_BT \simeq (R_{\text{eq}}^{\text{good}}/R_0)^{5-m}$ and $F_{\text{ternary}}(R_0)/k_BT \simeq (R_{\text{eq}}^{\Theta_s}/R_0)^{8-2m}$. Hence $R_{\text{eq}}^{\Theta_s} > R_0$ when $F_{\text{ternary}}(R_0) \gg k_BT$. The inequality $x^a > y^b$ implies $x > y$ if $x > 1$, $y > 1$ and $a < b$. Accordingly, $F_{\text{binary}}(R_0) > F_{\text{ternary}}(R_0)$ implies $R_{\text{eq}}^{\text{good}} > R_{\text{eq}}^{\Theta_s}$ because $5 - m < 8 - 2m$. Note that the opposite inequality $x^a < y^b$ only implies $x < y^{b/a}$ which does not exclude $x > y$. In a poor solvent $R_{\text{eq}}^{\text{poor}} > R_0$ is possible though $R_{\text{eq}}^{\text{poor}} < R_0$ is a prerequisite for a collapse transition.

IV. Applicability Range of the Theory and the Scaling Regimes

The scaling laws reported above are applicable subject to inequalities enforcing the underlying assumptions and the packing constraints. Some of the requirements apply also to linear chains and their brushes: The Gaussian extension elasticity $F_{\text{el}}/kT \simeq (R/R_0)^2$ is only applicable when $gs \gg 1$ though it is reasonable approximation when $gs > 3$. Approximating the interaction free energy by the second and third virial terms implies $\phi_{\text{eq}} \ll 1$. As already noted, swollen regimes with $R_{\text{eq}} > R_0$ occur when $F_{\text{interaction}} \gg k_BT$. However, for dendron brushes it is also necessary to impose (i) $R_{\text{max}} > R_{\text{eq}} > R_{\text{min}}$ to allow for packing constraints (ii) $R_{\text{eq}} \gg R_{\text{min}}$ so as to ensure $\phi_{\text{eq}} \ll 1$ and the applicability of the virial expansion, (iii) the inequalities required for the various solvent regimes such as $F_{\text{binary}}(R_0) \gg F_{\text{ternary}}(R_0)$ for good solvent, or $F_{\text{ternary}} \gg k_BT$ for Θ_s solvent; the latter condition is never fulfilled for linear chains. In addition our scaling analysis applies to brushes of crowded dendrons when $R_0 > \delta$ and to semiflexible chains with $p \ll s$ (Appendix B). These requirements, the packing constraints in particular, narrow the scaling regimes of dendronized brushes as compared to these of "normal" brushes.

For comparison purposes it is helpful to express the inequalities in terms of the triple R: R_{min}, R_0, and R_{max}. This automatically ensures a common description applicable to both dendronized and normal brushes. In this presentation the two systems differ because the accessible range of R_{min}, R_0, and R_{max} is much smaller for dendronized brushes because of packing constraints manifested by g_{max}. This is illustrated for the athermal solvent with $\tau = 1$ in Figures 5 and 6. The effect of τ variation on the scaling regimes of DP ($m = 1$) is depicted in Figure 7. All state diagrams contain significant regions where the scaling regimes do not apply. A similar though weaker effect occurs also for linear chains.

The triple R plots bring out certain common features of dendronized and normal brushes. However, this presentation hides useful design information regarding the effect of s, p, g, δ, X, or f. To explore these trends it is helpful to depict the scaling regimes in g, p, s plots as illustrated in Figure 8 showing the good and Θ_s regions for the case of $X = 3$ and tethered dendrons at $\tau = 1$ and $\delta = 5b$. On the basis of information gathered from such plots (cf. ref 62), the following trends emerge: Both the poor and good solvent regimes broaden with increasing $|\tau|$ and s. Similarly, for $m > 0$, the boundaries of both regimes broaden with δ/b. The poor solvent range is independent of p since it is determined by the interplay of F_{binary} and F_{ternary}. In contrast, the boundaries of the good solvent and Θ_s regions do depend on p because they reflect the interplay of $F_{\text{interaction}}$ and the p-dependent F_{el}. Θ_s regimes can occur for both positive and negative τ. Its boundaries broaden as $|\tau|$ increases but shrink as δ/b increases. While the boundaries of the Θ_s regions depend on p, the dependence is weaker than in the good solvent regimes. The good solvent regime decreases in size with increasing m for a constant δ. It also decreases with increasing X due to the corresponding decrease in g_{max}. Importantly, for all solvent regimes the accessible g range is rather narrow, even for relatively large s. For the spacers considered, with $1 \le s \le 10$, the widest g range is of order 10 and is typically narrower. The narrowness of the good solvent scaling windows is due, in part, to the relatively fast growth of R_{min} with n. In particular, it increases faster than $R_{\text{eq}}^{\text{good}}$ for $m < 2$ and faster than $R_{\text{eq}}^{\Theta_s}$ for $m = 0$.

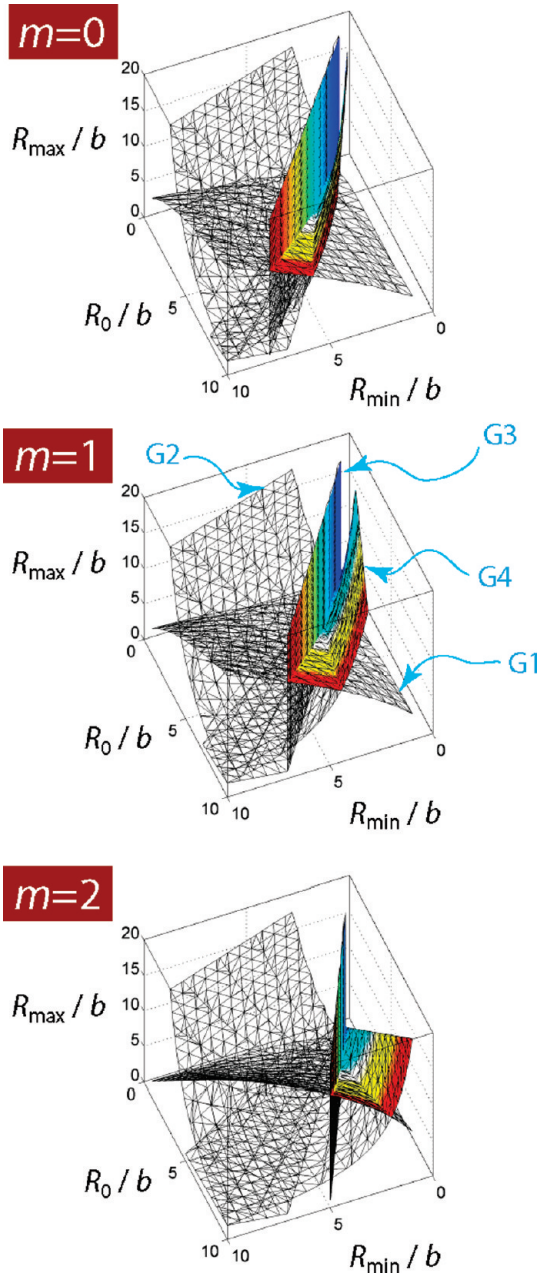

Figure 6. Additional information about the left column of Figure 5, here for a slightly different solvent quality, $\tau = {}^1/_2$. For each m (from dendron, $m = 0$, to dendronized forest, $m = 2$) all four meshes corresponding to the inequalities G1−G4 are shown. The actual scaling window has to respect all inequalities and is thus bound by these surfaces. Similarly, the Θ_s and poor solvent regimes are obtained by considering inequalities T1−T5 and P1−P2.

The state diagrams depicted concern a particular choice of parameters. They highlight however a general difficulty in discriminating scaling laws due to two features: (a) The narrowness of the domains where the scaling laws apply (b) the occurrence of relatively broad crossover regions. The state diagrams are thus helpful for the design of simulations and experiments aiming to probe scaling behavior. A utility generating state diagrams for arbitrary parameters is available.[62]

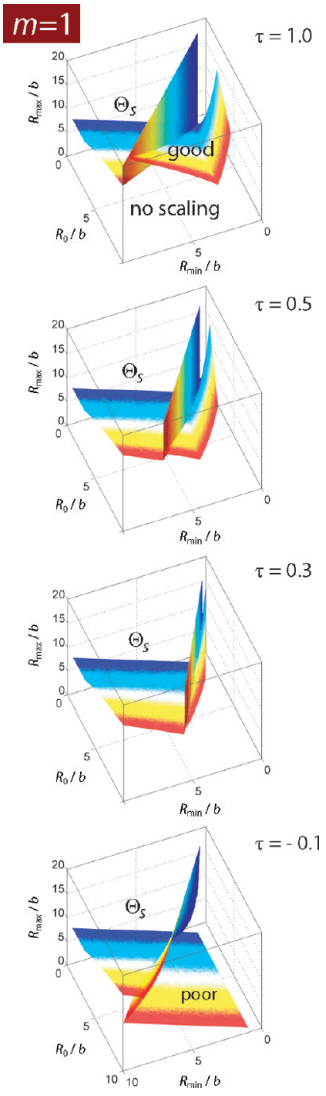

Figure 7. Effect of solvent quality on the triple R state diagram and size of the good, Θ_s and poor solvent regimes for $m = 1$ (dendronized polymers), from $\tau = 1$ (top) to $\tau = -0.1$ (bottom). The region where scaling behavior is absent is partially accessible within packing constraints, because it extends into the region where $R_{max} > R_{min}$, most easily seen at $\tau = -0.1$ (the diagonal plane limiting the poor solvent regime toward low R_{max} has $R_{max} = R_{min}$). For free linear chains, $R_{min} < R_0$ holds, and thus renders the Θ_s regime inaccessible.

V. Collapse

The free energy, eq 11, can not fully describe the collapse behavior when $R_0 > R_{min}$. To explore the possibility of a collapse transition it is necessary to replace $F_{el}/k_BT \simeq (R/R_0)^2$ by F_{el} allowing also for confinement to $R < R_0$. To this end our discussion follows the analysis of the collapse transition as carried out by Birshtein and Pryamitsyn[58] utilizing earlier results by Fixman.[59] It invokes a numerical approximation of the Fixman result (see Appendix C)

$$\frac{F_{el}}{k_BT} \simeq \left(\frac{R}{R_0}\right)^2 - 3\left(\frac{R}{R_0}\right)^{1/3} + \frac{2}{5}\left(\frac{R_0}{R}\right)^{5/2} \qquad (18)$$

enabling the study of $F_{strand} = F_{el} + F_{binary} + F_{ternary}$ as a function of the swelling ratio $\alpha \equiv R/R_0$ defined in terms of the radius of gyration

$$\frac{F_{strand}}{k_BT} \simeq \alpha^2 - 3\alpha^{1/3} + \frac{2}{5}\alpha^{-5/2} + \tau B\alpha^{m-3} + C\alpha^{2m-6} \qquad (19)$$

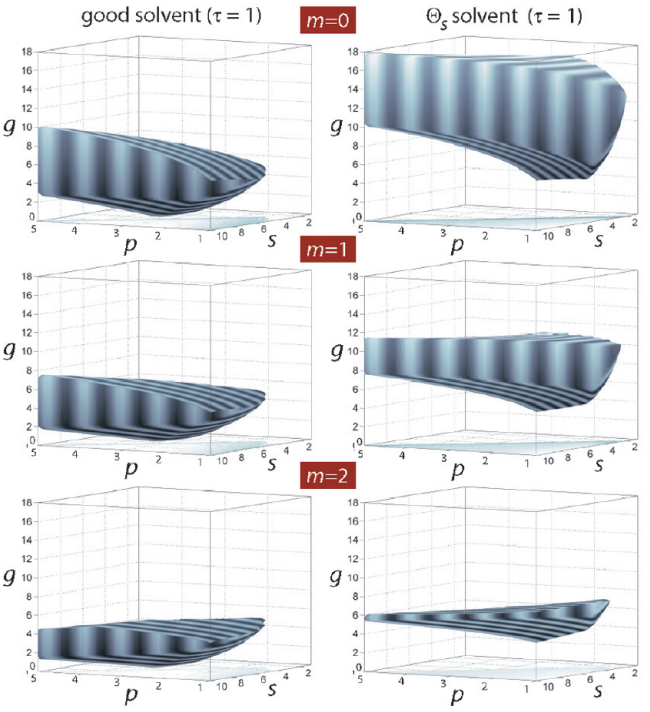

Figure 8. Left column: Particular representation of the more general triple R state diagrams (cf. Figure 5), again for all surface dimensionalities m (increasing from top to bottom) at $\tau = 1$. The particular choice is $X = 3, f = 1$ (free or tethered three-functional dendron), and $\delta = 5b$ so that the scaling diagram can be drawn in terms of generation g, spacer length s, and persistence length $\sim p$. Corresponding results for Θ_s scaling are shown in the right column. The two regions have a common, curved boundary. With decreasing τ the volume for the good solvent scaling regime shrinks (not shown) with concurrent growth of the Θ_s regime, as the geometrical bounds are unaffected by τ. With increasing functionality X the geometrical bound is decreasing further.

Here $\tau B = F_{binary}(R_0)/k_BT$ and $C = F_{ternary}(R_0)/k_BT$ are explicitly specified, using eqs 12 and 13, by

$$B \simeq \frac{(ns)(b/\delta)^m}{(gs)^{(1-m)/2}} p^{-(3-m)/2}, \quad C \simeq \frac{B^2}{gs} \qquad (20)$$

B and C can also be expressed conveniently in terms of the triple R's, cf. eq A1 of Appendix A:

$$B \simeq \left(\frac{R_{max}}{b}\right) C, \quad C \simeq \left(\frac{R_{min}}{R_0}\right)^{6-2m} \left(\frac{R_{max}}{b}\right) \qquad (21)$$

For given τB and C the equilibrium swelling ratio α_{eq} is specified by minimizing F_{strand} (eq 19) with respect to α, for each m, subject to the relevant constraints: $R_{min} < R_{eq} < R_{max}$, or $(C/B)^{1/(3-m)} < \alpha_{eq} < B(pC)^{-1/2}$, as well as $R_0 > \delta$ (see Appendix B for further considerations concerning solvent quality). Equation 19 describes brushes of both dendrons and of linear chains depending on the choice of B and C as well as the imposed constraints.

We note in passing that it is common practice to base the discussion on the equilibrium condition, $dF_{strand}/d\alpha = 0$

$$\alpha_{eq}{}^5 - \frac{1}{2}(\alpha_{eq}{}^{10/3} + \alpha_{eq}{}^{1/2}) = \tau B\alpha_{eq}{}^m + C\alpha_{eq}{}^{2m-3} \qquad (22)$$

Equation 22 is useful for analytical calculations and approximations. It is also of interest because it is the equilibrium condition invoked previously.[7,58] From this point of view note that in these papers the left-hand side of eq 22 is approximated by $\alpha_{eq}{}^5 - \alpha_{eq}{}^3$

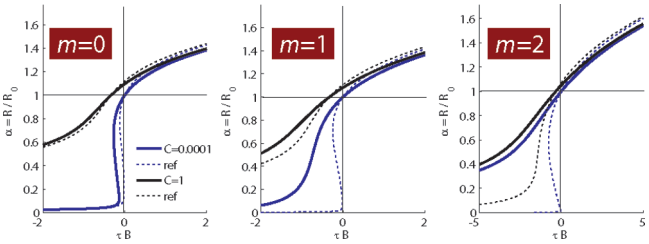

Figure 9. The ratio $\alpha = R/R_0$ obtained from eq 22 for all three surface dimensionalities, m. The exact numerical result, cf. Appendix C, is also plotted, but not visible as it coincides with our approximate result based on eq C5. The broken reference lines are the predictions based on the approximation proposed in ref 58. B and C are specified in eq 20.

and $(9/\pi^2)(\alpha_{eq}{}^3 - \alpha_{eq})$ for $\tau > 0$ and $\tau < 0$ which perform poorly around $\tau = 0$ (Figure 9). In the case of dendron brushes, where packing constraints are especially important, the solution of eq 22 may fail to capture the accessible minimum free energy state. Furthermore, from a practical point of view the use of eq 22 to investigate the collapse transition requires anyhow a numerical solution. Altogether, eq 22 is thus of limited utility.

The general features of the collapse behavior are discernible from the unconstrained α_{eq} vs τB plots (Figure 9). These are obtained by minimizing eq 19 without imposing packing constraints. They thus describe brushes of both dendrons and of linear chains but may contain physically inaccessible regions specific to each system. With these caveats the plots suggest that a first order collapse transition is possible for star polymers and dendrimers ($m = 0$). For dendrimers this scenario was already suggested on the basis simulations utilizing a coarse-grained model.[51] For DP and bottle brushes $m = 1$the conditions for a first order collapse are unlikely to be satisfied. For DP the collapse transition occurs for C of the order of $C \leq 10^{-4}$. In turn, this requires $ns\delta/b < p^{1/2}R_0/b$ or $n < g^{1/2}s^{-1/2}pb/\delta$ corresponding to short and stiff spacers and low line density ensuring however $R_0 > \delta$. These conditions are not satisfied for high-generation dendrons with $n \gg g$. Furthermore, they are not satisfied in experimentally known systems. Thus, for a homologous series of vinyl-type dendronized polymers, with $3 \leq g \leq 5$, for which $\delta/b \approx 1$, $s \approx 6$, $p \approx s/2$, and $X = 3$,[11] both C and $gs^{-1/2}pb/\delta$ are of order unity for all g and thus suggesting a continuous collapse. For forests and planar brushes there is no indication of first order collapse transition (Figure 9).

VI. Discussion and Conclusions

Our discussion of dendron brushes invokes the assumption that all monomers are spheres of diameter b with identical virial coefficient. This commonly used view is justified in part by the lack of data concerning the solubility, interactions and dimensions of the different monomeric species: junctions, spacers and ends. With this caveat, the theory yields qualitative insights concerning dendron brushes in general and allows confrontation with simulations where this assumption can be rigorously imposed. The scaling laws of the equilibrium span of dendron brushes are summarized in Table 1 and their regimes of applicability are depicted in Figures 5, 7, and 8. Our results suggest the continuous collapse in DP and forests and a possibility of first order collapse transition in dendrimers.

On every topic considered, the formulation immediately allows to compare dendron brushes with brushes of linear chains as well between brushes of different m. In particular, our expressions (see Table 1) reduce to the known case of linear chains and their brushes upon setting $g = 1, n = f$, and identifying the number of monomers in a grafted chain with s.[63,64] The scaling behavior of brushes of linear chains is by now well-established, cf. reviews[2,63,65,66] and[13,14,32,33,43,44,67] for recent examples.

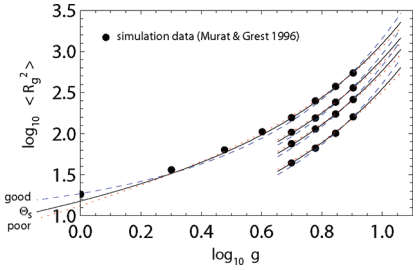

Figure 10. Mean square radius of gyration vs g as obtained in[49] for three-functional dendrimers ($m = 0, f = X = 3$) with flexible spacers ($s = 7, p \approx 1$). Shown are scaling predictions according to all three regimes tabulated in Table 1. The data does not allow to discriminate between the different scaling laws apart from incompatibility with the Θ_g case. Simulations at constant ns and for different gs or vice versa would help to test the scaling predictions unambiguously (see Table 2).

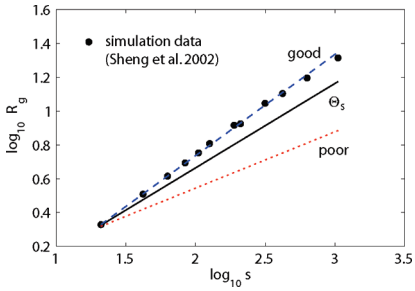

Figure 11. Double-logarithmic plot of radius of gyration vs spacer length s of the data obtained in ref 9 of $g = 2$ dendrimers ($m = 0$, $f = X = 3$) with flexible spacers, varying s at constant p. The data set does allow to discriminate between the different scaling laws in this particular representation not shown in the original article.

Importantly, our analysis highlights the practical difficulties in validating the dendron brushes scaling laws with respect to n and g. These arise because of the narrowness of the "scaling windows", the width of crossover regions and the mutual dependence of the scaling variables n and g. This last issue comes up when comparing our results to simulations of dendron brushes. Most of the effort to discriminate scaling laws concerned dendrimers ($m = 0$). The experimental and simulation data is typically considered to be consistent with scaling behavior.[27] However, the conclusions are not always clear-cut. The difficulties are illustrated by an example. The data may be consistent with different scaling laws as illustrated in Figure 10 using the data of Murat and Grest (MG).[49] Similar conclusions were also reached in.[8,46,48] This example is balanced by sets of data that do allow distinguishing between different scaling regimes. A case to the point is the data of ref 9 as re-plotted in Figure 11. This figure shows simulation data for the radius of gyration of dendrimers versus spacer length at otherwise unchanged conditions, including fixed g. The scaling analysis confirms that the systems under investigation had been subjected to good solvent conditions. Another prominent example where scaling exponents could be obtained unambiguously is the work by Chen and Cui[68] who studied star-burst dendrimers made of hard sphere chains of fixed bond length, varying sphere diameter, g and s. Comparison with our results requires identifying the three characteristic sizes; cf. footnote 69 for details. As noted above, re-analyzing the MG results (Figure 10) demonstrates that the data can be fitted by all three scaling expressions for dendrimers, cf. Table 1. Using our classification for the solvent conditions, the MG simulations were carried out within the Θ_s scaling window (see footnote 70). Our discussion suggests that a better discrimination can be attained upon comparing systems with either identical ns, or identical gs. Thus, it would be particularly helpful to compare $m = 0$

Table 2. Architectures Exhibiting Similar $R_{min}/b \simeq ns$ but Significantly Different Equilibrium Sizes, $R_{eq}^{\Theta_s}$, for the Case of Flexible Dendrimers ($m = 0, p = 1$,)[a]

R_{min}/b	f	X	s	g	n	R_0/b	R_{max}/b	$R_{eq}^{\Theta_s}/b$	$R_{eq}^{\Theta_s}/R_{min}$
4.3	3	4	2	3	39	2.4	6.0	4.7	1.09
4.3	3	3	9	2	9	4.2	18.0	6.2	1.43
6.3	2	3	2	6	135	3.5	12.0	7.4	1.17
6.3	3	3	12	3	21	6.0	36.0	9.8	1.55
8.8	2	5	4	4	170	4.0	16.0	10.2	1.16
8.8	2	3	11	5	62	7.4	55.0	13.9	1.58
10.1	3	5	4	4	255	4.0	16.0	11.3	1.12
10.0	2	3	8	6	126	6.9	48.0	14.8	1.48
10.3	3	4	3	5	363	3.9	15.0	11.3	1.10
10.4	3	3	12	5	93	7.7	60.0	16.1	1.55
10.8	3	5	5	4	255	4.5	20.0	12.6	1.17
10.8	2	3	10	6	126	7.7	60.0	16.6	1.54

[a] This is achieved upon variation of X, s, and g, whereas n and the characteristic sizes are obtained from eqs 1, 5, 6, 10, and 15. The table assumes $\tau = 1$. This choice does not imply good solvent scaling since the inequalities in eqB2 imply that all listed examples belong to the swollen Θ_s scaling regime.

dendrimers with identical $R_{min} \sim (ns)^{1/3}$ but with different s, X, or f and with significantly different $R_{max} \simeq gsb$. The effect of these parameters is illustrated by examples for the case of dendrimers ($m = 0$) in Table 2. For $m > 0$, including DPs, the situation is conceptually simpler because the continuous variable δ can be used to adjust R_{min}. The research activity concerning the younger fields of forests and dendronized polymers lags behind that of the better-established dendrimers. It faces the same problems discussed earlier for the dendrimers. The confrontation with scaling laws requires extended homologous series within the scaling window and with judicious variation of the molecular design parameters. To our knowledge this challenge is not yet fulfilled.

Acknowledgment. We thank A. D. Schlüter for helpful comments. M.K. acknowledges financial support through the Swiss National Science Foundation grant IZ73Z0-128169 and ETH Research Grant ETH-17 10-1.

Appendix A: Scaling in Terms of Characteristic Dimensionless Sizes

The explicit results we obtained for the "identical monomer" scenario, scaling laws and inequalities are expressed in terms of n, g, s, b, p, and δ. These can be also expressed in terms of R_{min}, R_0, R_{max}, and b, a formulation of interest for plotting the results in a system-independent fashion. To this end, note that only R_{min} depends on n while solely R_0 contains p. To obtain scaling laws in terms of R_{min}, R_0, and R_{max} we can follow the following procedure: (i) ignore s, b and δ (ii) replace n by ${R_{min}}^{3-m}$, p by ${R_0}^2/R_{max}$, g by R_{max}, and (iii) ensure the proper dimensions by multiplying with an appropriate power of b. For example, the dimensionless factor $ng^2s^3p(b/\delta)^m$ in R_{eq}^{good} is first transformed into ng^2p using (i) which is transformed into ${R_{min}}^{3-m}({R_0}^2/R_{max}){R_{max}}^2 = {R_{min}}^{3-m}{R_0}^2R_{max}$ using (ii) and multiplied by b^{6-m} because of (iii) thus leading to the identity $ng^2s^3p(b/\delta)^m = {R_{min}}^{3-m}{R_0}^2R_{max}b^{m-6}$. In particular, we obtain, with $\tau B = F_{binary}(R_0)/k_BT$ and $C = F_{ternary}(R_0)/k_BT$ as introduced in eq 19

$$\frac{F_{eq}^{good}}{k_BT} \simeq \tau({R_{min}}^{6-2m}{R_0}^{2m-6}{R_{max}}^2/b^2)^{1/(5-m)} = \tau B^{2/(5-m)}$$
$$\frac{F_{eq}^{\Theta_s}}{k_BT} \simeq ({R_{min}}^{6-2m}{R_0}^{2m-6}R_{max}/b)^{1/(4-m)} = C^{1/(4-m)} \quad \text{(A1)}$$
$$\frac{F_{eq}^{poor}}{k_BT} \simeq \tau^2 R_{max}/b$$

Appendix B: Applicability Windows and Scaling Diagrams

State diagrams delineating the boundaries of the scaling regimes are obtainable by implementing the inequalities required for the good, Θ, and poor solvent cases. Our discussion of state diagrams invokes two approaches. In one we express all quantities in terms of the triple R, i.e., R_{min}, R_0, and R_{max}. The resulting state diagrams, Figures 5, 7, are valid for any choice of physical parameters X, f, p and g, at a given τ and m. These types of diagrams allow to compare qualitative features of a broad class of systems at the price that the effect of specific parameters is not clearly discernible. To address these specific effects we resort to the second approach and plot g vs s and p in Figure 8. Notice that our discussion applies when $R_0 > \delta$ for $m > 0$ and all solvent qualities. Accordingly the relevant part of a triple R diagram is bound by $R_0 = \delta$.

1. Good Solvent. The applicability range for the good solvent scaling, eq 14, is limited by four inequalities, G1: $R_{eq}^{good} \ll R_{max}$, G2: $R_{eq}^{good} \gg R_{min}$, G3: $F_{binary}(R_0) \gg F_{ternary}(R_0)$, and G4: $F_{binary}(R_0) \gg k_BT$. In the triple R form these inequalities assume the form

$$\begin{aligned} &\text{G1}: && {R_{min}}^{m-3}{R_0}^{-2}{R_{max}}^{4-m}b &&\gg \tau \\ &\text{G2}: && {R_{min}}^{2}{R_0}^{-2}{R_{max}}^{-1}b &&\ll \tau \\ &\text{G3}: && {R_{min}}^{3-m}{R_0}^{m-3} &&\ll \tau \\ &\text{G4}: && {R_{min}}^{m-3}{R_0}^{3-m}{R_{max}}^{-1}b &&\ll \tau \end{aligned} \quad \text{(B1)}$$

In terms of physical tuning parameters, the same set of inequalities leads to

$$\begin{aligned} &\text{G1}: && (gs)^{3-m}(p\tau)^{-1} &&\gg (ns)(b/\delta)^m \\ &\text{G2}: && (gs)^{3-m}(p\tau)^{(3-m)/2} &&\gg (ns)(b/\delta)^m \\ &\text{G3}: && (gsp)^{(3-m)/2}\tau &&\gg (ns)(b/\delta)^m \\ &\text{G4}: && (gs)^{(1-m)/2}p^{(3-m)/2}\tau^{-1} &&\ll (ns)(b/\delta)^m \end{aligned}$$

These inequalities can only be satisfied when $\tau > 0$. For $m = 0$, the inequalities simplify to the following: G1, $\tau \ll n^{-1}g^3s^2/p$; G2, $\tau \gg n^{2/3}g^{-2}s^{-4/3}/p$; G3, $\tau \gg ng^{-3/2}s^{-1/2}p^{-3/2}$; G4, $\tau \gg n^{-1}g^{1/2}s^{-1/2}p^{3/2}$. For flexible linear chains ($n = g = p = 1$), inequalities G1 to G3 are fulfilled when G4 is fulfilled, that is, G4, $s \gg 1/\tau^2$, is the dominant constraint.[64]

2. Θ_s Solvent. The applicability range for the Θ_s (swollen Θ) scaling, eq 15, is determined by the inequalities T1: $R_{eq}^{\Theta_s} \ll R_{max}$, T2: $R_{eq}^{\Theta_s} \gg R_{min}$, T3: $F_{ternary}(R_0) \gg k_BT$, T4: $F_{ternary}(R_0) \gg F_{binary}(R_0)$, and T5: $F_{binary}(R_0) > -k_BT$. In the triple R representation the state diagram corresponds to

$$\begin{aligned} &\text{T1}: && {R_{min}}^{2m-6}{R_0}^{-2}{R_{max}}^{7-2m}b &&\gg 1 \\ &\text{T2}: && {R_{min}}^{-2}{R_0}^{2}R_{max}/b &&\gg 1 \\ &\text{T3}: && {R_{min}}^{6-2m}{R_0}^{2m-6}R_{max}/b &&\gg 1 \\ &\text{T4}: && {R_{min}}^{3-m}{R_0}^{m-3} &&\gg \tau \\ &\text{T5}: && {R_{min}}^{3-m}{R_0}^{m-3}R_{max}/b &&> (-\tau)^{-1} \end{aligned} \quad \text{(B2)}$$

whereas the explicit version is

$$\begin{aligned} &\text{T1}: && (gs)^{3-m}p^{-1/2} &&\gg (ns)(b/\delta)^m \\ &\text{T2}: && (gs)^{3-m}p^{(3-m)/2} &&\gg (ns)(b/\delta)^m \\ &\text{T3}: && (gs)^{1-m/2}p^{(3-m)/2} &&\ll (ns)(b/\delta)^m \\ &\text{T4}: && (gsp)^{(3-m)/2}\tau &&\ll (ns)(b/\delta)^m \\ &\text{T5}: && (gs)^{(1-m)/2}p^{(3-m)/2}(-\tau)^{-1} &&< (ns)(b/\delta)^m \end{aligned}$$

These inequalities can be satisfied for a range of negative and positive τ around $\tau = 0$. For free linear chains T3 reduces

to $p^{3/2} \ll 1$ and thus cannot be satisfied. For stars, the validity of T3 requires $f \gg p^{3/2}$. Note, that for linear chains the left hand sides of T1, T3−T5 decrease with increasing p. With exception of T4 at $m = 0$ the left hand sides of T1−T5 do not decrease with s. With the exception of free linear chains all systems may thus exhibit Θ_s scaling.

3. Θ_g Solvent. The applicability range for Θ_g scaling, $R_{eq} \simeq R_0$, is determined by the inequalities I1: $F_{ternary}(R_0) \ll k_BT$, and I2: $|F_{binary}(R_0)| \ll k_BT$,

$$\begin{array}{lrcl} \text{I1}: & {R_{min}}^{6-2m} {R_0}^{2m-6} R_{max}/b & \ll & 1 \\ \text{I2}: & {R_{min}}^{m-3} {R_0}^{3-m}/b R_{max} & \gg & |\tau| \end{array} \quad \text{(C6)}$$

Notice that I1 is the opposite of T3, and I2 similar to G4, so that there is no need to write down the corresponding explicit versions of the inequalities. For free linear chains, I1 is satisfied, but I2 is only valid for $|\tau| \ll p^{3/2}s^{-1/2}$. For stars, I1: $f^2 \ll p^3$ and I2: $|\tau| \ll p^{3/2}s^{-1/2}/f$. Accordingly, fully flexible f−functional stars should never exhibit Θ_g scaling behavior. Fully flexible linear chains do exhibit Θ_g for sufficiently small $|\tau| \sim s^{-1/2}$, and the $|\tau|$−range for Θ_g scaling is increasing with chain stiffness, while $s \gg p$ holds. For dendrimers, a valid inequality I2 requires very stiff spacers. For dendron brushes, Θ_g scaling could potentially be observed at small surface density, large p, and low g.

4. Poor Solvent. Finally, the applicability range for the poor solvent scaling is specified by $-1 < \tau < 0$, or $R_{eq}^{poor} \gg R_{min}$ in eq 17, and the additional inequalities P1: $R_{eq}^{poor} \ll R_{max}$ and P2: $F_{binary}(R_0) \ll -k_BT$, leading to

$$\begin{array}{lrcl} \text{P1}: & R_{max}{R_{min}}^{-1} & \gg & (-\tau)^{-1/(3-m)} \\ \text{P2}: & {R_{min}}^{3-m} {R_0}^{m-3} R_{max}/b & \ll & (-\tau)^{-1} \end{array} \quad \text{(B4)}$$

or

$$\begin{array}{ll} \text{P1}: & (gs)^{3-m}(-\tau) \gg (ns)(b/\delta)^m \\ \text{P2}: & (gs)^{(1-m)/2} p^{(3-m)/2} (-\tau)^{-1} \ll (ns)(b/\delta)^m \end{array}$$

These inequalities yield a lower limit for τ in the range $[-1,0]$. The poor solvent range of dendron brushes quickly diminishes with g and X. It is however broadened by increasing s and decreasing δ. For dendronized polymers, $m = 1$, the second inequality becomes $|\tau| \gg n^{-1}(p/s)(\delta/b)$, hence irrelevant, even for small $|\tau|$.

Appendix C: The Elastic Free Energy of a Linear Strand

The collapse behavior is characterized in terms of the swelling parameter $\alpha_{av} = R_{av}/R_0$ where $R_{av} = \langle R^2 \rangle^{1/2}$ and $\langle\rangle$ denotes an ensemble average. The key ingredients of the Birshtein−Pryamitsyn (BP) analysis[58] of the collapse transition concerns the choice of the α. Two issues are involved. The first concerns the choice of R. Defining α in terms of the end-to-end distance is misleading because $\alpha < 1$ may correspond to a loop rather to globule. A R defined in terms of the positions of all monomers rather than the two ends should provide a better characteristic of the volume occupied by the chain. This suggests the radius of gyration and the hydrodynamic radius. For practical reasons to be discussed shortly the radius of gyration is more convenient. The second issue concerns the choice of the distribution function specifying R_{av} and α. The BP analysis utilizes ${\alpha_{av}}^2 = \langle \alpha^2 \rangle = \int \alpha^2 p(\alpha^2)\, d\alpha^2$ with $p(\alpha^2)$ normalized via $\int p(\alpha^2)\, d\alpha^2 = 2\int p(\alpha^2)\alpha\, d\alpha = 1$. This choice plays an important role because the resulting moment generating function for the radius of gyration exhibits the form of a Laplace transform yielding an explicit relationship between the elastic force f_{el} and α_{av}. A similar approach is not possible for $\tilde{p}(\alpha)\, d\alpha$ normalized $\int \tilde{p}(\alpha)\, d\alpha = 1$ or $4\pi \int \alpha^2 \tilde{p}(\alpha)\, d\alpha = 1$.

The required $p(\alpha^2)$ can be simply discussed in terms of the maximum entropy prescription. In particular, we maximize the entropy $-k_B \int p(\ln(p/p_0))\, d\alpha^2$ subject to two constraints: (i) the normalization condition $\int p_0(\alpha^2)\, d\alpha^2 = 1$; (ii) an imposed value of ${\alpha_{av}}^2$. It is accordingly necessary to minimize the functional $S/k_B = -\int p(\ln(p/p_0))\, d\alpha^2 - \ln(G/e) - \lambda {\alpha_{av}}^2 = -\int p[\ln(p/p_0) + \ln(G/e) + \lambda\alpha^2]\, d\alpha^2$ where G and λ are the α-independent Lagrange parameters corresponding to the constraints and p_0 is the probability distribution function of an unperturbed random walk such that $\int p_0(\alpha^2)\, d\alpha^2 = 1$ and $\int \alpha^2 p_0(\alpha^2)\, d\alpha^2 = 1$. Note that the explicit form of p_0 for the radius of gyration is unknown though it is available for the end-to-end distance. We return to this point later. The distribution $p(\alpha^2)$ is specified by the minimum condition as obtained be the variational derivative of S with respect to p: $\delta S[p]/\delta p = -k_B[\ln(p/p_0) + 1 + \ln G + \lambda\alpha^2] = 0$ yielding $p(\alpha^2) = G^{-1} p_0 \exp(-\lambda\alpha^2)$. The normalization condition then specifies the partition function

$$G(\lambda) = \int_0^\infty p_0(\alpha^2) \exp(-\lambda\alpha^2)\, d\alpha^2 \quad \text{(C1)}$$

or $G = \int_0^\infty p_0(s) \exp(-\lambda s)\, ds$. This G with $G(0) = 1$, is the Laplace transform of p_0 and it can formally be inverted to yield p_0 via a Bromwich integral of G. Hence, $G(\lambda)$ is also the moment-generating function of p and the second moment of p, ${\alpha_{av}}^2$, is given by ${\alpha_{av}}^2 = -G^{-1}\, dG/d\lambda = -d(\ln G)/d\lambda$. Accordingly, given an explicit form for $G(\lambda)$ or $p_0(\alpha^2)$ it is possible to obtain α_{av} in terms of λ. For the case of the radius of gyration of a random walk, Fixman[59] obtained the explicit form of $G(\lambda)$ in the limit of long chains upon expressing the radius of gyration in terms of segments and its distribution function as a product of distribution functions for segments, In particular $G(\lambda) = (z^{-1} \sin z)^{-3/2}$, with $z = (-4\lambda)^{1/2}$, or equivalently $G(\lambda) = [2\lambda^{-1/2} \sinh(2\lambda^{1/2})]^{-3/2}$ thus leading to ${\alpha_{av}}^2 = -d(\ln G)/d\lambda$,

$${\alpha_{av}}^2 = -\frac{3}{4\lambda}[1 - 2\lambda^{1/2} \coth(2\lambda^{1/2})] \quad \text{(C2)}$$

Equation C2 has solutions only for $\lambda \geq -\pi^2/4$ corresponding to $G \leq \pi$. For small $|\lambda|$, ${\alpha_{av}}^2 = 1 - 4\lambda/15 + o(\lambda^2)$ is close to unity (see also ref 72) while in the limit of large positive λ, $\coth(2\lambda^{1/2}) \approx 1$ and ${\alpha_{av}}^2 \approx (3/2)\lambda^{-1/2}$.

To relate F_{el} to λ and α_{av} we consider the free energy $F = -TS = k_BT \int p(\ln(p/p_0))\, d\alpha^2 = A - \int \lambda\alpha^2 p\, d\alpha^2 = A - k_BT\lambda {\alpha_{av}}^2$. Here $A = -k_BT(\ln G)$ is a Helmholtz free energy which does not explicitly depend on ${\alpha_{av}}^2$ while the elastic free energy $F_{el} = -k_BT\lambda {\alpha_{av}}^2$ expresses λ in terms of F_{el} and α_{av}. Specifying the dimensionless elastic force defined by $f_{el} \equiv d(F_{el}/k_BT)/d\alpha_{av}$

$$\lambda = -\frac{f_{el}}{2{\alpha_{av}}^2} \quad \text{(C3)}$$

Combining eq C3 in eq C2 and utilizing $ix \coth(ix) = x \cot(x)$ leads to

$${\alpha_{av}}^2 = \frac{3\alpha_{av}}{2f_{el}}\left[\alpha_{av} - (2f_{el})^{1/2} \cot\left(\frac{2f_{el}}{{\alpha_{av}}^2}\right)^{1/2}\right] \quad \text{(C4)}$$

a non nonlinear relationship between f_{el} and α_{av} which we would like to solve for f_{el} in terms of α_{av}. For small f_{el} the right-hand side of eq C4 becomes $1 + 2f_{el}/15{\alpha_{av}}^2$; hence, $\alpha_{av} = 1 + f_{el}/15 + o(f_{el}^2)$. For large positive f_{el} one can have $f_{el} \sim {\alpha_{av}}^2$ at most, because λ has a lower bound noted earlier. For large negative f_{el}, λ tends to

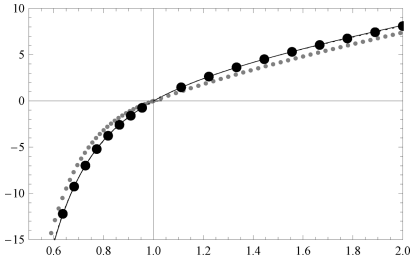

Figure 12. f_{el} versus α. Exact numerical result according to eq 19 (solid line), Approximate expressions were proposed in ref 58 (small dots) and eq C5 (large dots).

be large and positive, so that $\alpha_{av}{}^2 \approx \lambda^{-1/2} \sim (\alpha_{av}{}^2/f_{el})^{1/2}$, hence $f_{el} \sim \alpha_{av}{}^{-2}$. Earlier treatments have approximated f_{el} by using a simple interpolation formula recovering the limiting cases. However, this approach does not perform well at the vicinity of $\alpha_{av} = 1$, a range of special importance for dendron brushes because α has both lower and upper bounds given by R_{min}/R_0 and R_{max}/R_0. A better performance is achieved by an accurate approximation for the solution of eq C2,

$$f_{el} \approx \frac{\pi^2}{2}\alpha_{av}\left(1 - \frac{1}{2}\left[\alpha_{av}{}^{-5/3} + \alpha_{av}{}^{-9/2}\right]\right) \qquad \text{(C5)}$$

as demonstrated in Figure 12 for $\alpha \geq -0.6$ showing, in addition, the approximations suggested and applied in.[58] The elastic entropy corresponding to eq C5 is obtained by integration over α thus leading to

$$F_{strand}^{el}/k_BT \approx \frac{\pi^2}{4}\left(\alpha_{av}{}^2 - 3\alpha_{av}{}^{1/3} + \frac{2}{5}\alpha_{av}{}^{-5/2}\right)$$

used in eq 18. This F_{strand}^{el} exhibits a minimum at $\alpha = 1$ as it should and shows almost perfect quantitative performance, down to $\alpha \ll 1$, as demonstrated in Figure 9. The asymptotic behavior of eq 18 in the limit of vanishing α is however different from the correct expression $F_{strand}^{el}/k_BT = (9/4)(\alpha^{-2} + 2\ln\alpha)$ of BP.[58] On the other hand eq 18 correctly recovers the $\alpha \gg 1$ limit $F_{strand}^{el}/k_BT = (\pi^2/4)$-$(\alpha^2 - 2\ln\alpha)$.

For α defined in terms of the end-to-end distance, the case usually treated in textbooks,[61,64] p_0 is analytically known, $p_0 \sim \alpha^y \exp(-\gamma\alpha^2)$ with $\gamma = 3/2$ and $y = 1$. The second moment of p_0 should be identical to unity ($\alpha_0 = R_0/R_0 = 1$). Performing Gaussian integrals, one obtains $\int\alpha^2 p_0\, d\alpha^2/\int p_0\, d\alpha^2 = (1+2)/3 = (2+y)/3$, confirming $y = 1$. Insertion of p_0 into eq C2 yields $\alpha_{av}{}^2 = 3/(3+2\lambda)$. Equation C1 evaluates as $G(\lambda) \sim (1+2\lambda/3)^{-3/2}$, so that $\alpha_{av}{}^2 = -d\ln G/d\lambda = 3/(3+2\lambda)$. Using the relationship between λ and f_{el} from eq C4 the expression for $\alpha_{av}{}^2$ can be also written as $\alpha_{av}{}^2 = 3/(3 - f_{el}/\alpha_{av})$, or equivalently, $f_{el} = 3(\alpha_{av} - \alpha_{av}{}^{-1})$ or $F_{el}/k_BT = 3\alpha/2 - 3\ln\alpha$. These are the classical results for the case that α stands for the end-to-end distance, whereas eq C5 can be used for the case that α represents the dimensionless gyration radius.

The ideas outlined in this appendix had been generalized to anisotropic situations, including liquid crystals[73,74] and flow-induced anisotropy,[75] and play a role in nonequilibrium thermodynamics,[73,76] where one assumes a generalized canonical distribution function, and determines an entropy expression from a consistently measured Lagrange parameter−friction matrix pair through a combination of biased Monte Carlo and short-time molecular dynamics.[75,76]

References and Notes

(1) Newkome, G. R.; Moorefield, C. N.; Vögtle, F. *Dendrimers and dendrons*; Wiley-VCH: Weinheim, Germany, 2001.
(2) Milner, S. T. *Science* **1991**, *251*, 905.
(3) Vögtle, F.; Richardt, G.; Werner, N.; Rackstraw, A. J. *Dendrimer Chemistry: Concepts, Syntheses, Properties, Applications*; Wiley-VCH: Weinheim, Germany, 2009.
(4) Tomalia, D. A.; Naylor, A. M.; Goddard, W. A. *Angew. Chem., Int. Ed.* **1990**, *29*, 138–175.
(5) Fréchet, J. M. J.; Tomalia, D. A. *Dendrimers and Other Dendritic Polymers*; John Wiley & Sons: New York, 2001.
(6) Benhabbour, S. R.; Sheardown, H.; Adronov, A. *Macromolecules* **2008**, *41*, 4817.
(7) Boris, D.; Rubinstein, M. *Macromolecules* **1996**, *29*, 7251.
(8) Giupponi, G.; Buzza, D. M. A. *J. Chem. Phys.* **2004**, *120*, 10290.
(9) Sheng, Y.-J.; Jiang, S.; Tsao, H.-K. *Macromolecules* **2002**, *35*, 7865.
(10) Klos, J. S.; Sommer, J.-U. *Macromolecules* **2009**, *42*, 4878–4886.
(11) Guo, Y.; van Beek, J.; Zhang, B.; Colussi, M.; Walde, P.; Zhang, A.; Kröger, M.; Halperin, A.; Schlüter, A. D. *J. Am. Chem. Soc.* **2009**, *131*, 11841.
(12) Carlmark, A.; Hawker, C.; Hult, A.; Malkoch, M. *Chem. Soc. Rev.* **2009**, *38*, 352–362.
(13) Sheiko, S. S.; Möller, M. *Chem. Rev.* **2001**, *101*, 4099.
(14) Pyun, J.; Kowalewski, T.; Matyjaszewski, K. *Macromol. Rapid Commun.* **2003**, *24*, 1043.
(15) Schlüter, A. D.; Rabe, J. P. *Angew. Chem., Int. Ed.* **2000**, *39*, 864.
(16) Tatarinova, E. A.; Rebrov, E. A.; Myakushev, V. D.; Meshkova, I. B.; Demchenko, N. V.; Bystrova, A. V.; Lebedeva, O. V.; Muzafarov, A. M. *Russ. Chem. Bull.* **2004**, *53*, 2591–2600.
(17) Frauenrath, H. *Prog. Polym. Sci.* **2005**, *30*, 325.
(18) Schlüter, A. D. *Top. Curr. Chem.* **2005**, *245*, 151.
(19) Lee, C. C.; MacKay, J. A.; Fréchet, J. M. J.; Szoka, F. C. *Nat. Biotechnol.* **2005**, *23*, 1517.
(20) Frauenrath, H. *Prog. Polym. Sci.* **2005**, *30*, 235–384.
(21) Zhang, A. F.; Shu, L. J.; Bo, Z. S.; Schlüter, A. D. *Macromol. Chem. Phys.* **2003**, *204*, 328–339.
(22) Östmark, E.; Macakova, L.; Auletta, T.; Malkoch, M.; Malmström, E.; Blomberg, E. *Langmuir* **2005**, *21*, 4512.
(23) Tokuhisa, H.; Zhao, M.; Baker, L. A.; Phan, V. T.; Dermody, D. L.; Garcia, M. E.; Peez, R. F.; Crooks, R. M.; Mayer, T. M. *J. Am. Chem. Soc.* **1998**, *120*, 4492.
(24) Xiao, Z.; Cai, C.; Mayeux, A.; Milenkovic, A. *Langmuir* **2002**, *18*, 7728.
(25) Ornelas, C.; Ruiz, J.; Belin, C.; Astruc, D. *J. Am. Chem. Soc.* **2009**, *131*, 590.
(26) Laus, S.; Sour, A.; Ruloff, R.; Toth, E.; Merbach, A. *Chem.—Eur. J.* **2005**, *11*, 3064.
(27) Ballauff, M.; Likos, C. N. *Angew. Chem., Int. Ed.* **2004**, *43*, 2998–3020.
(28) Percec, V.; Heck, J.; Tomazos, D.; Falkenberg, F.; Blackwell, H.; Ungar, G. *J. Chem. Soc. Perk T.* **1993**, *1*, 2799.
(29) Li, Z.; Yu, G.; Wu, W.; Liu, Y.; Ye, C.; Qin, J.; Li, Z. *Macromolecules* **2009**, *42*, 3864.
(30) Xiao, S.; Fu, N.; Peckham, K.; Smith, B. D. *Org. Lett.* **2010**, *12*, 140.
(31) Popa, I.; Longtin, R.; Maroni, P.; Papastavrou, G.; Borkovec, M. *Chimia* **2009**, *63*, 279.
(32) Lecommandoux, S.; Checot, F.; Borsali, R.; Schappacher, M.; Deffieux, A. *Macromolecules* **2002**, *35*, 8878–8881.
(33) Wintermantel, M.; Gerle, M.; Fischer, K.; Schmidt, M.; Wataoka, I.; Urakawa, H.; Kajiwara, K.; Tsukahara, Y. *Macromolecules* **1996**, *29*, 978.
(34) Rathgeber, S.; Pakula, T.; Wilk, A.; Matyjaszewski, K.; Beers, K. L. *J. Chem. Phys.* **2005**, *122*, 124904.
(35) Lee, W. B.; Elliott, R.; Mezzenga, R.; Fredrickson, G. H. *Macromolecules* **2009**, *42*, 849–859.
(36) Welch, P. M.; Welch, C. F. *Nano Lett.* **2006**, *6*, 1922–1927.
(37) Rodriguez-Ropero, F.; Canales, M.; Zanuy, D.; Zhang, A.; Schlüter, A. D.; Aleman, C. *J. Phys. Chem. B* **2009**, *113*, 14868–14876.
(38) Ding, Y.; Kröger, M. *Macromolecules* **2009**, *42*, 576–579.
(39) Kröger, M.; Peleg, O.; Ding, Y.; Rabin, Y. *Soft Matter* **2008**, *4*, 18–28.
(40) Ding, Y.; Öttinger, H. C.; Schlüter, A. D.; Kröger, M. *J. Chem. Phys.* **2007**, *127*, 094904.
(41) Christopoulos, D. K.; Terzis, A. F.; Vanakaras, A. G.; Photinos, D. J. *J. Chem. Phys.* **2006**, *125*, 204907.
(42) Connolly, R.; Bellesia, G.; Timoshenko, E. G.; Kuznetsov, Y. A.; Elli, S.; Ganazzoli, F. *Macromolecules* **2005**, *38*, 5288–5299.
(43) Bishop, M.; Clarke, J. H. R. *J. Chem. Phys.* **1989**, *90*, 6647.
(44) Huissmann, S.; Blaak, R.; Likos, C. N. *Macromolecules* **2009**, *42*, 2806–2816.

(45) Hunter, R. J. *Foundations of Colloid Science*; Clarendon: Oxford, U.K., 1986; Vol. I.
(46) Karatasos, K.; Adolf, D. B.; Davies, G. R. *J. Chem. Phys.* **2001**, *115*, 5310–5318.
(47) Wallace, E. J.; Buzza, D. M. A.; Read, D. J. *Macromolecules* **2001**, *34*, 7140–7146.
(48) Scherrenberg, R.; Coussens, B.; van Vliet, P.; Edouard, G.; Brackman, J.; de Brabander, F.; Mortensen, K. *Macromolecules* **1998**, *31*, 456–461.
(49) Murat, M.; Grest, G. S. *Macromolecules* **1996**, *29*, 1278–1285.
(50) Cavallo, L.; Fraternali, F. *Chem.—Eur. J.* **1998**, *4*, 927–934.
(51) Timoshenko, E. G.; Kuznetsov, Yu.A.; Connolly, R. *J. Chem. Phys.* **2002**, *117*, 9050–9062.
(52) Hsu, H. P.; Paul, W.; Binder, K. *J. Chem. Phys.* **2008**, *129*, 204904.
(53) Batsoulis, J.; Kremer, K. *Europhys. Lett.* **1988**, *7*, 683.
(54) Efthymiopoulos, P.; Vlahos, C.; Kosmas, M. *Macromolecules* **2009**, *42*, 1362–1369.
(55) Ding, Y.; Kröger, M. *J. Comput. Theor. Nanosci.* **2010**, *7*, 1–14.
(56) Efthymiopoulos, P.; Kosmas, M.; Vlahos, C.; Gergidis, L. N. *Macromolecules* **2007**, *40*, 9164.
(57) Denesyuk, N. A. *Phys. Rev. E* **2003**, *67*, 051803.
(58) Birshtein, T. M.; Pryamitsyn, V. A. *Macromolecules* **1991**, *24*, 1554.
(59) Fixman, M. *J. Chem. Phys.* **1962**, *36*, 306.
(60) For the case of fully flexible spacers, $p = 1$, a linear chain corresponds also to a strand of g bifunctional $X = 2$ junctions joined by single bonds, $s = 1$, such that $n = g$.[11] For the case of semiflexible spacers, $p > 1$, a strand of g bifunctional $X = 2$ junctions joined by spacers of length s corresponds to a piecewise semiflexible linear chain. The homogeneous semiflexible linear chain with s bonds in total is captured by $g = 1$ and $n = 1$.
(61) De Gennes, P.-G. *Scaling Concepts in Polymer Physics*, 3rd ed.; Cornell University Press: London, 1988. See also references cited therein.
(62) Add on material for this manuscript is available online at http://www.complexfluids.ethz.ch/scaling
(63) Halperin, A.; Tirrell, M.; Lodge, T. P. *Adv. Polym. Sci.* **1992**, *100*, 31–71.
(64) Rubinstein, M.; Colby, R. H. *Polymer Physics*; Oxford University Press: Oxford, U.K., 2003.
(65) Szleifer, I.; Carignano, M. A. *Adv. Chem. Phys.* **1996**, *94*, 165–260.
(66) Advincula, R. C.; Brittain, W. J.; Caster, K. C.; Rühe, J. *Polymer brushes: Synthesis, characterization, applications*; Wiley-VCH: Weinheim, Germany, 2004.
(67) Zhulina, E. B.; Birshtein, T. M. *Polym. Sci. USSR* (*Engl. Transl.*) **1985**, *27*, 570.
(68) Chen, Z. Y.; Cui, S. M. *Macromolecules* **1996**, *29*, 7943.
(69) For a flexible hard sphere chain with bond studied in,[68] the maximum bending angle is $\theta_{max} = \cos^{-1}(d^2/4 - 1)$, and the mean bending angle is $\langle\cos\theta\rangle = \cos(\theta_{max}/2)^2$. Our dimensionless persistence p length is thus approximated by the result for a freely rotating chain with constant bending angle, $p = (1 + \langle\cos\theta\rangle)/(1 - \langle\cos\theta\rangle) = (4 + d^2)/(4 - d^2)$ which reduces to $p = 1$ for $d = 0$ and to $p = {}^5/_3$ for $d = 1$. For the systems studied in ref 68, $R_{max} = lgs$, $R_0 = (gsp)^{1/2}l$, and $R_{min} = (d/2)(\phi_m ns)^{1/3}$, where $\phi_m = 0.638$ might be well approximated by the volume fraction of the maximally random jammed state, cf. ref 71. That is, R_{max} and R_0 are compatible with the choice $b = l = 1$, but b in eq 6 depends on d.
(70) The simulated dendrimers in ref 49 are characterized by $m = 0$, $s = 7$, $b = 1$, $X = f = 3$, and $p \approx 1$. Corresponding characteristic sizes are, e.g., $R_{min} \approx 6.8$ (22.1), $R_0 \approx 4.4$ (7.3), and $R_{max} \approx 20.4$ (54.3) for $g = 3$ ($g = 8$) according to eqs 6, 10, and 5, respectively. These values, as well as corresponding ones for generations $g \leq 8$ studied in ref 49, validate the inequalities T1−T5 of eq B2 for $\tau = 1$. Thus the system corresponds to Θ_s conditions, where the ternary interactions control the swelling of this athermal system.
(71) Foteinopoulou, K.; Karayiannis, N. C.; Laso, M.; Kröger, M.; Mansfield, M. L. *Phys. Rev. Lett.* **2008**, *101*, 265702.
(72) Flory, P. J.; Fisk, S. J. *J. Chem. Phys.* **1971**, *55*, 4338.
(73) Beris, A. N.; Edwards, B. J. *Thermodynamics of flowing systems with internal microstructure*: Oxford Science: Oxford, U.K., 1993.
(74) Ilg, P.; Karlin, I. V.; Kröger, M.; Öttinger, H. C. *Physica A* **2003**, *319*, 134–150.
(75) Ilg, P.; Öttinger, H. C.; Kröger, M. *Phys. Rev. E* **2009**, *79*, 011802.
(76) Öttinger, H. C. *Beyond equilibrium thermodynamics*; Wiley: Hoboken, NJ, 2005.